energies

MDPI

Article

ANN for Temperature and Irradiation Prediction and Maximum Power Point Tracking Using MRP-SMC

Mokhtar Jlidi [1,2], Oscar Barambones [2,*], Faiçal Hamidi [1] and Mohamed Aoun [1]

[1] Laboratory Modélisation, Analyse et Commande des Systèmes, University of Gabes, Gabes LR16ES22, Tunisia; m.moktarjlidi@gmail.com (M.J.); faicalhamidi@yahoo.fr (F.H.); mohamed.aoun@macs.tn (M.A.)

[2] Automatic Control and System Engineering Department, University of the Basque Country, UPV/EHU, Nieves Cano 12, 01006 Vitoria-Gasteiz, Spain

* Correspondence: oscar.barambones@ehu.eus; Tel.: +34-94-501-3235; Fax: +34-94-501-3270

Abstract: Currently, artificial intelligence (AI) is emerging as a dominant force in various technologies, owing to its unparalleled efficiency. Among the plethora of AI techniques available, neural networks (NNs) have garnered significant attention due to their adeptness in addressing diverse challenges, particularly for prediction tasks. This study offers a comprehensive review of predominant AI-based approaches to photovoltaic (PV) energy forecasting, with a particular emphasis on artificial neural networks (ANNs). We introduce a revolutionary methodology that amalgamates the predictive capabilities of ANN with the precision control afforded by the minimum-risk problem and sliding mode control (MRP-SMC), thereby revolutionizing the PV panel performance enhancement. Building upon this methodology, our hybrid approach utilizes the ANN as a proficient weather forecaster, accurately predicting the temperature and solar radiation levels impacting the panels. These forecasts serve as guiding principles for the MRP-SMC algorithm, enabling the proactive determination of the Maximum Power Point (MPP). Unlike conventional methods that grapple with weather unpredictability, the MRP-SMC algorithm transforms stochastic optimization challenges into controllable deterministic risk problems. Our method regulates the boost converter's work cycle dynamically. This dynamic adaptation, guided by environmental predictions from ANNs, unlocks the full potential of PV panels, maximizing energy recovery efficiency. To train the model, we utilized a large dataset comprising 60,538 temperature and solar radiation readings from the Department of Systems Engineering and Automation at the Faculty of Engineering in Vitoria (University of the Basque Country). Our approach demonstrates a high regression coefficient (R = 0.99) and low mean square error (MSE = 0.0044), underscoring its exceptional ability to predict real energy values. In essence, this study proposes a potent fusion of artificial intelligence and control mechanisms that unleash the untapped potential of photovoltaic panels. By utilizing forecasts to guide the converter, we are paving the way for a future where solar energy shines brighter than ever.

Keywords: minimal risk problem; forecasting; ANN; SMC; MPPT; boost

Citation: Jlidi, M.; Barambones, O.; Hamidi, F.; Aoun, M. ANN for Temperature and Irradiation Prediction and Maximum Power Point Tracking Using MRP-SMC. *Energies* **2024**, *17*, 2802. https://doi.org/10.3390/en17122802

Academic Editor: Adel Merabet

Received: 4 May 2024
Revised: 3 June 2024
Accepted: 4 June 2024
Published: 7 June 2024

1. Introduction

Renewable energies, with solar power at the forefront, are essential to meeting the challenge of a sustainable energy supply [1,2]. However, the unpredictable nature of sunlight prevents the full potential of solar energy from being exploited [3,4]. To overcome this problem, Maximum Power Point Tracking (MPPT) technology and reliable weather forecasts optimize the PV system efficiency and energy production [5,6]. MPPT ensures that solar panels operate at maximum power under varying sunlight conditions [7,8]. Accurate weather forecasts allow proactive adjustments to MPPT algorithms and system operations [9,10]. The integration of MPPT technology and reliable weather forecasts significantly improves the energy yield and efficiency of solar installations [11,12]. These advances pave the way for a sustainable solar-powered energy future [13,14].

Conventional MPPT algorithms, such as Perturb and Observe (P&O), Hill Climbing (HC), and Incremental Conductance (IC), often struggle to efficiently track the Maximum Power Point (MPP) under stochastic conditions [15,16]. These limitations can lead to significant energy losses and reduced system efficiency [17,18].

Advanced MPPTs such as particle swarm optimization (PSO) and JAYA outperform but are not well-suited to addressing large and complex optimization challenges and are prone to triggering at local optima [19,20]. PSO can converge prematurely to sub-optimal solutions [21], while JAYA's sensitivity to initial conditions and limited exploration of the search space can hamper its effectiveness [22]. The large search space inherent in the genetic algorithm (GA) parameter optimization process can significantly hamper the system speed and increase the complexity [23].

These limitations can lead to significant energy losses in solar energy systems, particularly in dynamic environments with fluctuating irradiance and partial shading [24].

This research addresses the challenge of optimizing operational processes under uncertainty by applying a methodology described in [25]. Stochastic optimization problems are addressed by transforming them into equivalent deterministic formulations, in particular, in scenarios with fully admissible solutions. The approach introduces a deterministic optimization problem presented as a minimum-risk problem (MRP), solved efficiently using non-linear mathematical programming methods. This methodology is then applied to derive optimal decision frameworks for simplified industrial applications, with a specific case study demonstrating the practical application in the optimization of solar energy systems.

In addition, the growing need to predict future trends in various fields has fuelled a strong demand for forecasting techniques. In this context, ANNs have emerged as powerful tools. ANNs have been successfully applied in various fields, including tourism (e.g., forecasting tourist numbers or hotel stays [26]), financial trading [27], and the energy sector (e.g., forecasting renewable energy production and energy consumption [28–30]). Numerous studies consistently demonstrate the superior performance of ANNs, particularly when dealing with high-frequency data, compared to traditional forecasting methods.

In [31], the performance of the ANN model was evaluated against various models documented in the literature, including Quadratic Support Vector Machine (QSVM), Decision Tree [32], Convolution Neural Network–Bi-Direction Long Short-Term Memory (CNN-BILSTM) [33], Deep Learning (DL) [34], Adaptive Neuron Fuzzy Inference System (ANFIS) [35], Group Method of Data Handling (GMDH) [36], and ANFIS-PSO [37], to predict different types of solar radiation. The evaluation used the Mean Squared Error (MSE) and regression(R) criteria to ensure a complete and accurate comparison. The results of this comparative analysis unequivocally demonstrated the superior accuracy of the ANN model compared with the aforementioned models. In particular, the study highlighted the challenges associated with determining hyper-parameters and specific parameters in the other models, a concern mitigated by the relative ease of implementation of the ANN model.

In many studies, researchers have frequently used the proportional integration (PI) controller to regulate the controller duty cycle. Specifically, in research [38], the Fuzzy-PI method was used for control and, in another study [39], a combination of ANN and PI was implemented. Despite the effectiveness of the PI controller, it faces challenges related to its inherent linearity, which complicates its applicability to non-linear systems, as well as the tuning complexities associated with selecting optimal parameters. Alternatively, sliding mode control (SMC) is emerging as a robust and versatile control method recognized for its ability to handle uncertainties and disturbances in dynamic systems.

Many approaches have been explored by researchers to improve the efficiency of photovoltaic systems. In [40], the authors presented a PV-TE hybrid system, combining photovoltaic (PV) and thermal (TE) cells, as a solution to the energy efficiency problems of PV technology. In parallel, ref. [41] used a fuzzy method to find the Maximum Power Point (MPP), while [42] used mathematical models for gradient optimization specifically adapted to photovoltaic panels. Despite their effectiveness, these methods do not address stochastic

challenges due to the dynamic nature of the environment. Various prediction techniques, including physical methods, have been proposed, but they have some limitations. For example, as reported in [43], physical and indirect forecasting methods struggle to accurately predict future weather conditions. However, in [41], artificial intelligence emerged as a promising avenue for forecasting.

This paper presents significant advances in the applications of control systems for renewable energy sources. A key aspect of this work is taking advantage of artificial neural networks (ANNs) for temperature and solar radiation forecasting. The adoption of artificial neural networks is justified by their versatility and proven effectiveness in various domains, highlighting their suitability for this particular field. In addition, the paper proposes a new approach using the MRP-SMC method to control DC–DC converters, aligning with the essential principle of Maximum Power Point Tracking (MPPT). This innovative methodology improves converter performance, thus optimizing energy extraction in renewable energy systems.

This paper introduces two pivotal contributions to the field. First, it harnesses the power of artificial neural networks (ANNs) to accurately predict temperature and solar radiation levels, taking advantage of their well-established effectiveness in a multitude of domains. Secondly, it adopts an innovative MRP-SMC-based approach to control DC–DC converters according to the principles of Maximum Power Point Tracking (MPPT). The MRP method skillfully addresses the stochastic challenges arising from unpredictable weather conditions, while sliding mode control (SMC) excels in its ability to managing the uncertainties and disturbances inherent in dynamic systems. By seamlessly integrating these two methodologies, the paper improves the ability to explore the point of maximum power and precisely regulate the flow of energy within renewable energy systems. This holistic approach not only improves efficiency but also enhances the reliability of these systems, paving the way for sustainable energy solutions in the face of changing environmental dynamics.

The paper is structured as follows: Section 2 delves into the methodology, discussing the theoretical framework of the PV model and boost converter, as well as the predictive system and controllers utilized for MPPT. Section 3 outlines the neural-network-based predictive models employed, while Section 4 presents an analysis of the PV characteristics and controller performance. In Section 5, a comparative study is conducted between the proposed forecasting method and methods relying on the time series, alongside a comparison of the proposed MPPT method with the JAYA technique to evaluate the efficiency of the combined strategy. Finally, Section 6 concludes with a summary of the research's main achievements.

2. Methodology

Figure 1 illustrates the configuration of the examined system.

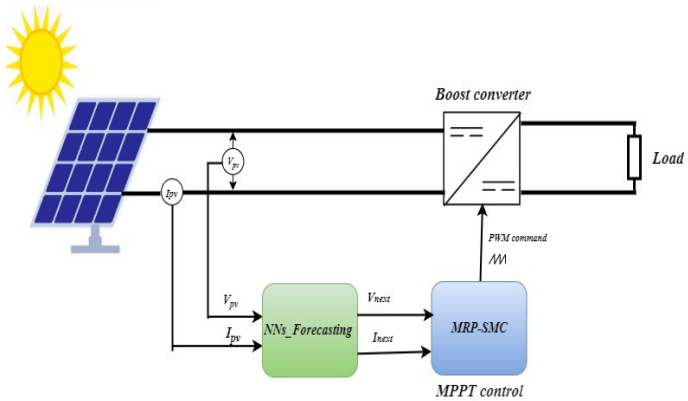

Figure 1. Study system.

2.1. PV Panel Modeling

The study employs the single-diode model due to its balance of accuracy and simplicity [44]. This model represents the photovoltaic (PV) system as a DC source within an electrical circuit, producing a current (Iph) from solar irradiation. It incorporates two types of resistances: Rsh, associated with the diode leakage current at the p-n junction [45], and Rs, which represents the resistance at the PV terminals [46]. Rs negatively affect the system's maximum power output [47]. Figure 2 illustrates the overall model.

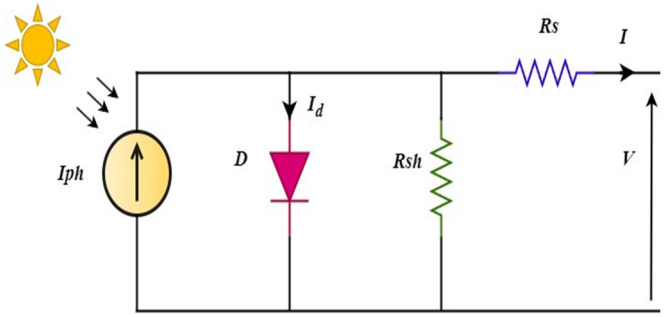

Figure 2. PV panel model.

The mathematical model (1) is derived from the equivalent circuit, representing a photovoltaic (PV) panel with N cells connected in series. While parallel connection of cells is possible, it is rarely seen in real-world scenarios.

$$I = I_{ph} - I_0\left(e^{\frac{q(V+IR_s)}{akTN_s}} - 1\right) - \frac{V + IR_s}{R_{sh}} \quad (1)$$

The initial expression represents the photocurrent, and is shown by Equation (2).

$$I_{ph} = G\frac{I_{sc} + K_i(T - T_{STC})}{G_{STC}} \quad (2)$$

G_{STC} and T_{STC} indicate radiation and temperature when tested under normal conditions. I_{SC} is the current in a short circuit, and K_i is the temperature coefficient.

$$I_0 = \frac{I_{sc} + K_i(T - T_{STC})}{e^{\frac{q(V_{OC} + K_v(T - T_{STC}))}{aKTN_s}} - 1} \quad (3)$$

The equations provided define some important terms: **q** is the constant representing electronic charge, $\mathbf{V_{oc}}$ is the open-circuit voltage, $\mathbf{K_V}$ is the temperature coefficient for open-circuit voltage, **a** is the solar ideal factor, **K** is Boltzmann's constant, and $\mathbf{N_S}$ is the number of series cells. Equation (2) shows that photocurrent is mainly affected by weather conditions like irradiation and temperature. Studies show that irradiation has a bigger effect on **Iph** than temperature, which ultimately influences the total current produced.

2.2. Hybrid MPPT Control

2.2.1. Boost Converter Model

This study used a boost converter to transfer energy from a solar panel to a resistive load. The boost converter increased the voltage from the solar panel to meet the needs of the load. A special boost topology was used for this purpose. Figure 3 shows how the boost converter was connected electrically.

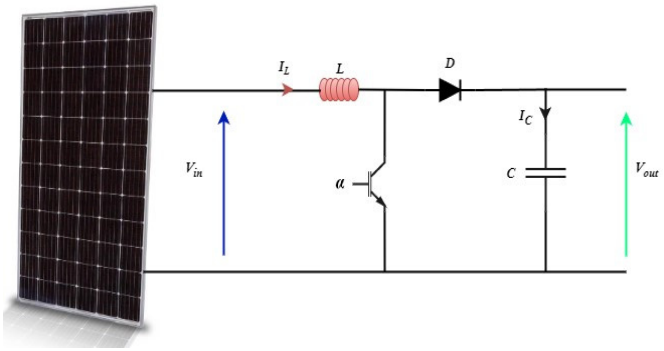

Figure 3. Boost converter's electrical diagram.

The duty cycle (α) determines the relationship between the input and output of the boost converter. This relationship appears in Equation (4). Controlled by a PWM signal generated by a MOSFET, it must be between 0.1 and 0.9 to maintain continuous conduction mode.

$$V_{out} = \frac{1}{1-\alpha} V_{in} \tag{4}$$

The state space representation of the boost converter uses two state variables: x1 for the input current and x2 for the output voltage.

$$\begin{cases} \dot{X} = \begin{bmatrix} 0 & \frac{\alpha-1}{L} \\ \frac{1-\alpha}{C} & \frac{-1}{RC} \end{bmatrix} \begin{bmatrix} x_1 \\ x_2 \end{bmatrix} + \begin{bmatrix} \frac{1}{L} \\ 0 \end{bmatrix} V_{in} \\ Y = \begin{bmatrix} 0 & 1 \end{bmatrix} \begin{bmatrix} x_1 \\ x_2 \end{bmatrix} \end{cases} \tag{5}$$

2.2.2. MRP-SMC Hybrid MPPT Control

1. The MPPT approach

Studying a PV panel trait, denoted as P = f(V), reveals how electrical power relies on the voltage it generates. The solar irradiance, symbolized by I_{rr}, underscores the changing nature of these energy sources. The subsequent expression illustrates a typical representation of a stochastic optimization problem (SOP):

$$\begin{aligned} &\max\left\{P(V) = C^T(I_{rr})f(V)\right\} \\ &\text{a.c.}: \begin{cases} A(I_{rr})V \leq b(I_{rr}) \\ V \geq 0 \end{cases} \end{aligned} \tag{6}$$

The main challenge of this SOP is dealing with uncertainty. We have three variable factors (**A**, **b**, and **C**) for each possible outcome in the events' space **Ω**. To find the optimal decision (**V***), we need to transform the problem into a defined format with acceptable solutions. This allows **V*** to account for all possible variations of **A** and **b**, ensuring that it is the best choice despite the randomness involved.

The initial formulation of the stochastic problem (6) can be replaced by an intermediate problem as shown in Equation (7) to address this complex problem by transforming it into a deterministic risk problem. This approach eliminates uncertainty by examining all possible scenarios and identifying the best decision for every situation. It simplifies technical terms, focusing on managing uncertainty and finding optimal solutions in complex scenarios.

$$\begin{cases} \min\{\alpha\} \\ \text{a.c.} \begin{cases} P\left(C^T f(V) < I_0\right) = \alpha \\ V \in D_{adm} \end{cases} \end{cases} \tag{7}$$

This problem aim to identify the option (V) that minimizes the risk of failing to achieve a target performance level (V_0). This target might be, for instance, the average value of a function (P(V)). Rather than directly minimizing the risk of failure, we focus on minimizing the probability associated with this risk. When a particular assumption about the random factor (c) is valid, we can transform this "minimal risk" problem into a more straightforward fixed problem. The solution to this simplified problem is given by the following equation:

$$\begin{cases} m_i = E(c_i) \\ u_{i,j} = E\left[(c_i - m_i)(c_j - m_j), U = (u_{i,j})\right] \end{cases} \tag{8}$$

A non-linear average optimization problem is considered:

$$\max\left\{P_{max} = m^T f(V)\right\} \tag{9}$$

The problem described in Equation (9) is deterministic, where the vector **m** represents the mean values $\mathbf{m_i}$, resulting in the solution $\mathbf{P^*_{max}}$ The function $\mathbf{P_{max}(V)}$ achieves its maximum value at $\mathbf{P_{max}^* = m^T f(V_{max}^*)}$, and we select $\mathbf{P_0 < P_{max}^*}$. The probability distribution of the random vector is approximated by a parabolic function with parameters $\mathbf{c_0}$, $\mathbf{c_1}$, and $\mathbf{c_2}$, where $\mathbf{P_{max}(V^*) = c_0V^2 + c_1V + c_2}$. Consequently, the outcomes are as follows:

$$\alpha = P_{ro}\left(C^T f(V) < P_0\right) = P_{ro}\left(\frac{C^T f(V) - m^T f(V)}{\sqrt{V^T U V}} < \frac{P_0 - m^T f(V)}{\sqrt{V^T U V}}\right) = \Phi\left(\frac{P_0 - m^T f(V)}{\sqrt{V^T U V}}\right) \tag{10}$$

In this context, $\boldsymbol{\alpha}$ represents the minimum risk, $\boldsymbol{\Phi}$ denotes the Laplace function, and $\mathbf{P_{ro}}$ stands for probability. In the earlier equation, **U** is the auto-covariance matrix of the $\mathbf{u_{i,j}}$ values from Equation (8). Because the Laplace function is monotonically increasing and the matrix **U** is positively definite, problem (10) simplifies into a straightforward optimization problem.

$$\min_{V \in D_{adm}} \left(\frac{P_0 - m^T f(V)}{\sqrt{V^T U V}}\right) \tag{11}$$

These problems can be addressed using conventional gradient methods in non-linear programming. This process includes choosing **V*** as the optimal solution for Equation (6). Additionally, Equation (11) matches Equation (12) in the context of maximization.

$$\max\left(\frac{m^T f(V) - P_0}{\sqrt{V^T \cdot U \cdot V}}\right) = \frac{c_0.V^2 + c_1.V + c_2 - P_0}{\sqrt{\begin{bmatrix} V^2 & V & 1 \end{bmatrix} U \begin{bmatrix} V^2 \\ V \\ 1 \end{bmatrix}}} \tag{12}$$

The solution to the problem, which corresponds to the voltage and current linked to the optimal operating point, was calculated using Rosen's Gradient.

2. Sliding Mode Controller

To determine the boost converter's duty cycle, we used SMC, a robust control algorithm that switches between states over time. This method effectively controls the input current without relying on specific system parameters and handles disturbances well. The selected sliding surface is as follows:

$$S = I_{ref} - I_{in} \tag{13}$$

The statement presents $\mathbf{I_{ref}}$ as the optimal current for MPPT control and $\mathbf{I_{in}}$ as the boost converter input current. It focuses on the application of a control law to guide the system on a sliding mode surface in finite time, by describing a specific structure for the control input.

$$U = U_{eq} - U_n \tag{14}$$

In the system, U_{eq}, representing the equivalent control input, governs the behavior on the sliding surface, while U_n, the non-linear switching input, directs and maintains the state on the sliding surface despite uncertainty. To obtain U_{eq} the initial condition is determined by ensuring $\dot{S} = 0$ [48].

$$\dot{S} = \dot{I}_{ref} - \dot{I}_{in} = 0 \tag{15}$$

where $\dot{I}_{in}$ is obtained from Equation (5), the boost converter state space

$$\begin{array}{l} \dot{I}_{ref} - \frac{1}{L}((U_{eq} - 1)V_{out} + V_{in}) = 0 \\ \Rightarrow U_{eq} = 1 - \frac{V_{in}}{V_{out}} \end{array} \tag{16}$$

By respecting and applying the Lyapunov criterion ($\dot{V} < 0$), U_n was obtained, with:

$$V = \frac{1}{2}S^2 \tag{17}$$

$$\dot{V} = S.\dot{S} < 0 \Leftrightarrow S.(-\frac{1}{L}((U - 1)V_{out} + V_{in})) < 0 \tag{18}$$

$$S.(-\frac{1}{L}((U_{eq} - U_n - 1)V_{out} + V_{in})) < 0 \Rightarrow S(\frac{-1}{L}U_n) < 0 \tag{19}$$

$$S.U_n > 0 \text{ where } U_n = k.sign(S) \tag{20}$$

The positive gain K is crucial: if too small, the controller loses robustness; if too large, it causes oscillations that can lead to chattering, or damage the control unit. Chattering can be reduced by replacing the "sign" function with a hyperbolic tangent function (tanh). Equation (21) presents the new control law.

Equation (21) describes the structure of the command law.

$$U = \frac{1}{2}(1 + \tanh(S)) \tag{21}$$

3. Neural-Network-Based Predictive Models

Artificial intelligence, especially NNs, is becoming more popular for forecasting because they are good at it. NNs work similarly to the brain, with interconnected parts that help them process information. They are being used in many industries, including forecasting, and they are showing great promise in making accurate predictions. The structure of the NN is represented in Figure 4.

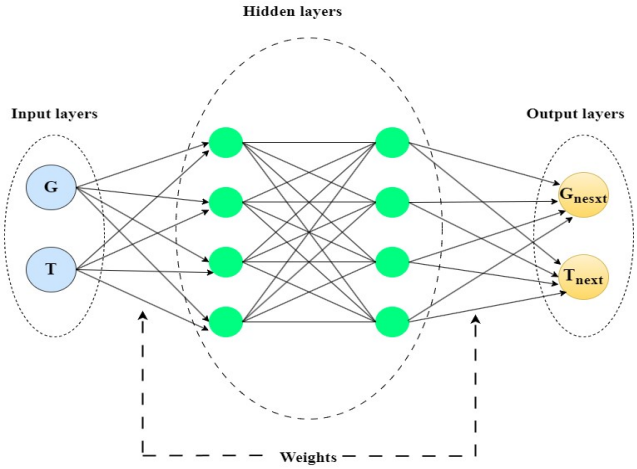

Figure 4. Neural network architecture.

The ANNs process information through a multi-layer architecture. The input layer receives the raw data, which are then transformed, and features are extracted in hidden layers using activation functions. The output layer produces the final prediction. The number of hidden layers, biases, and pooling layers are adjusted based on the complexity of the problem to improve performance. Customizing the network layers and neurons is crucial for each specific problem and dataset. This process is represented by Equation (22).

$$Y = \sigma(W_{i,j}{}^{T} * X_j - \beta) = \frac{1}{1 + e^{-(W_{i,j}{}^{T} * X_j - \beta)}} \tag{22}$$

$$W = \begin{bmatrix} w_{1,1} & \cdots & w_{1,j} \\ \cdot & \ddots & \cdot \\ \cdot & & \cdot \\ w_{i,1} & \cdots & w_{i,j} \end{bmatrix} \tag{23}$$

where

Y: the output layer;
σ: The activation function;
$\mathbf{W_{i,j}}$ represents the weight linking the i^{th} neuron in the preceding layer to the j^{th} neuron in the current layer;
$\mathbf{X_j}$: The output of the i^{th} neuron in the previous layer;
β: Biases.

To predict temperature and solar irradiance, we use an NN with the sigmoid activation function, which introduces non-linearity and ensures output values stay between 0 and 1, making it suitable for these continuous variables.

The process begins with data collection from the Department of Systems Engineering and Automation at Vitoria College of Engineering using a specialized sensor. The data are pre-processed, transformed, and standardized for input to the neural network. A statistical analysis informs the network design, which includes specific input, hidden, and output layers. The network is then trained using the efficient Scaled Conjugate Gradient (SCG) algorithm with adaptive learning rates and second-order optimization. Key metrics such as MSE and R monitor the training progress until the validation error stabilizes. Once trained, the network predicts the temperature and solar radiation (T and G) of new data. Rigorous validation and testing ensure accuracy and reliability, including partitioning data into training, validation, and test sets to adjust weights, prevent over-fitting, and objectively evaluate the performance. This approach ensures accurate forecasts. The following Figures 5 and 6 show the NN performance.

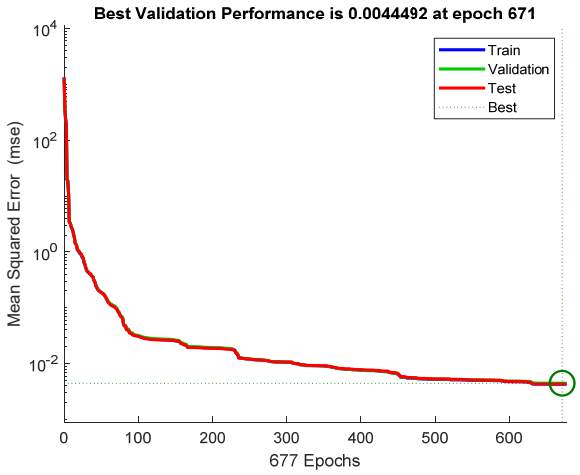

Figure 5. Mean square error.

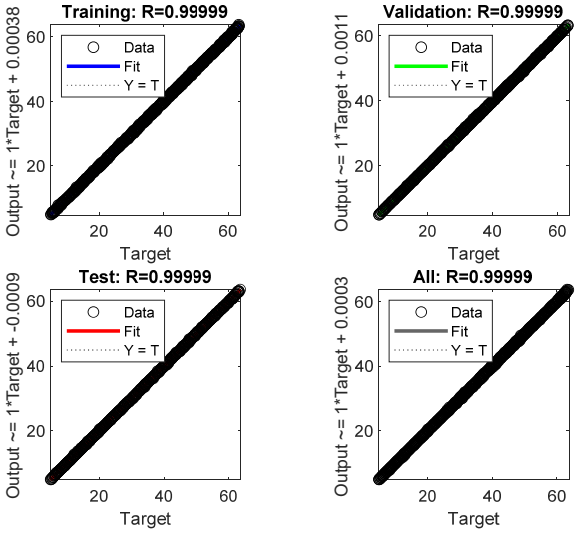

Figure 6. Regression.

During training, errors started repeating after 600 epochs, so the test was stopped at 677 epochs when the gradient was 0.0098. This repetition showed that the data were becoming more important. Epoch 200 was chosen as the baseline, and its weights were used as the final weights. Validation was carried out from Epoch 6 to 677, with errors repeating six times before stopping (see Figure 7).

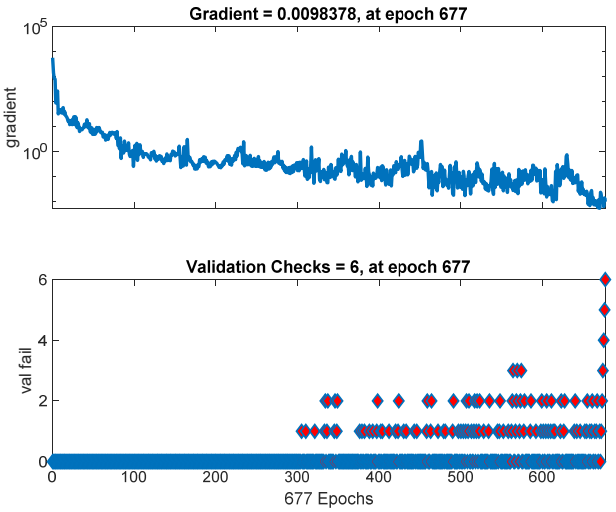

Figure 7. NN training.

From Figure 7, the red points represent the neural network's performance on the validation dataset at each epoch, while the blue line indicates its performance on the training dataset over the epochs.

Figure 8 illustrates the temperature and irradiance prediction outcomes, showcasing the efficacy of the proposed neural-network-based prediction methodology. Rigorously evaluated using real-world data, the technique undergoes a meticulous comparison between the experimental and predicted temperature, as well as irradiance values. The primary goal is to minimize the disparity between the anticipated outcomes and observed data. Encouragingly, a discernible alignment emerges between the predicted values and actual observations, signifying a robust agreement between the predictions and real results.

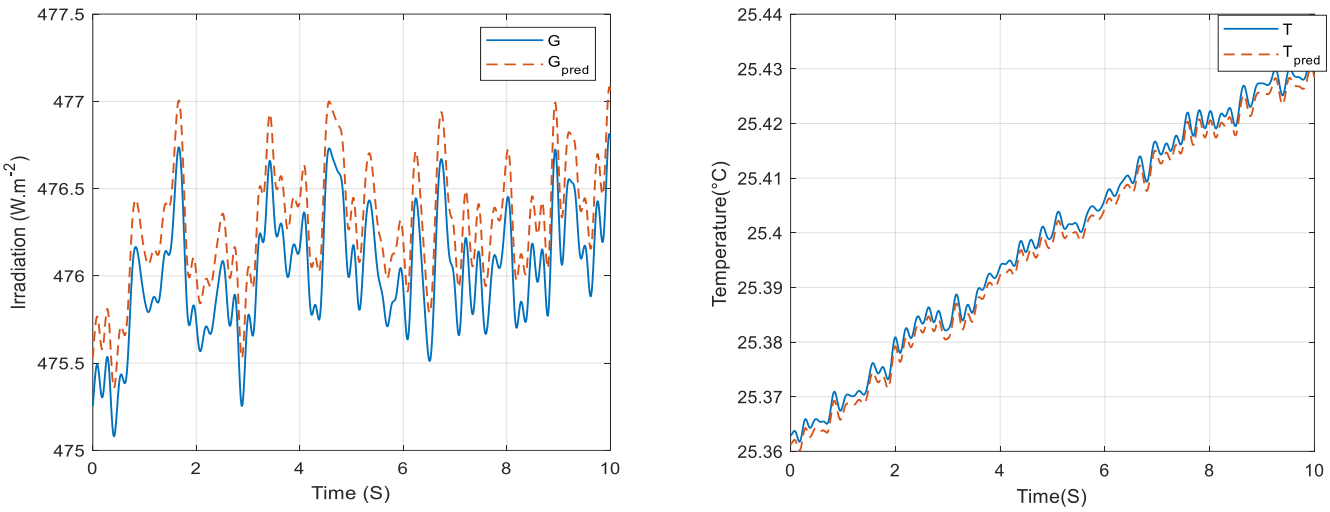

Figure 8. Prediction results.

An analysis of Figure 8 reveals a good agreement between the predicted values and observed results for temperature, with a minimum error of about 0.16 for solar radiation. The results confirm the reliability and robustness of the forecasting process, and confirm its effectiveness in capturing complex dynamics with a high degree of accuracy.

The efficacy of neural networks heavily relies on hyper-parameters. Previous studies, referenced as [48,49], have explored various techniques such as the Bayesian Gaussian substitution process, boosted gradient regression trees, random forest, and heuristic algorithms to identify optimal hyper-parameter configurations. In this current investigation, diverse neural network architectures underwent training and cross-validation. This process involved weight optimization using the back-propagation algorithm, while considering the impact of the number of epochs and hidden-layer NNs' performance.

Through experimentation, the most efficient configuration was determined to be a two-layer feedback network with 15 hidden-layer neurons, trained for 1000 epochs using the SCG algorithm. The dataset comprised 60,538 temperatures and solar radiation values, with 70% allocated to training and 30% to validation and testing sets. The network demonstrated its suitability for regression tasks, evidenced by an MSE of 0.0044 and R of 0.99, as depicted in Figures 5 and 6, respectively. These results indicate a strong correlation between the network's outcomes and the desired objectives, with minimal error.

4. Results

Appendices B and C detail the specifications of the SG340P PV panel and the boost converter, with a resistor used as the load. The initial step was to assess the SG340P panel's performance under various temperature and radiation levels. Figure 9 presents the IV and PV characteristics recorded under these different conditions.

The $\mathbf{P_{PV}}$ curve shows the power generated by the PV panel without tracking, while the $\mathbf{P_{MPP}}$ represents the maximum power achieved with the proposed tracking technique. Figure 11 demonstrates that the PV power curve does not reach its maximum potential. However, the strength of the MPP detection algorithm lies in its precise identification of the Maximum Power Point (MPP), even during sudden fluctuations, a challenge for other methods. This highlights its exceptional ability to adapt to dynamic conditions.

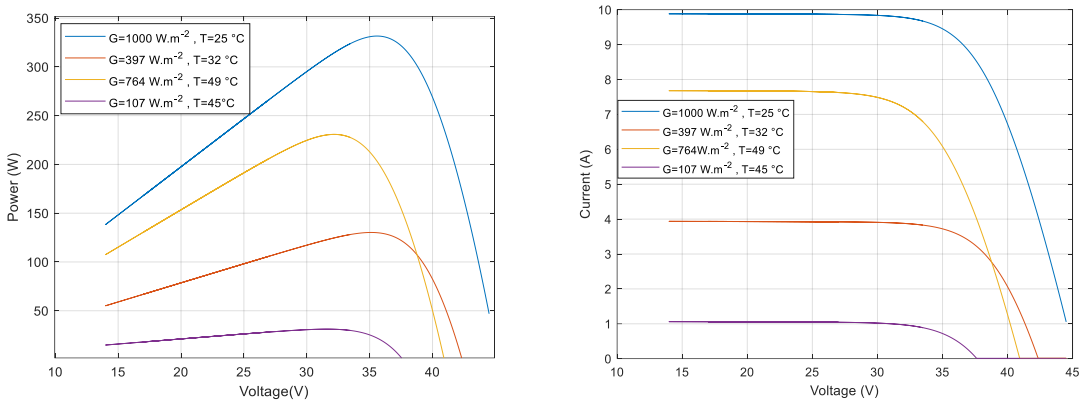

Figure 9. PV panel characteristics.

To accurately evaluate the performance of the Minimum-Risk Problem (MRP) algorithm under different conditions, we conducted a series of tests at different levels of temperature and solar radiation. Figure 10 provides details of the test parameters.

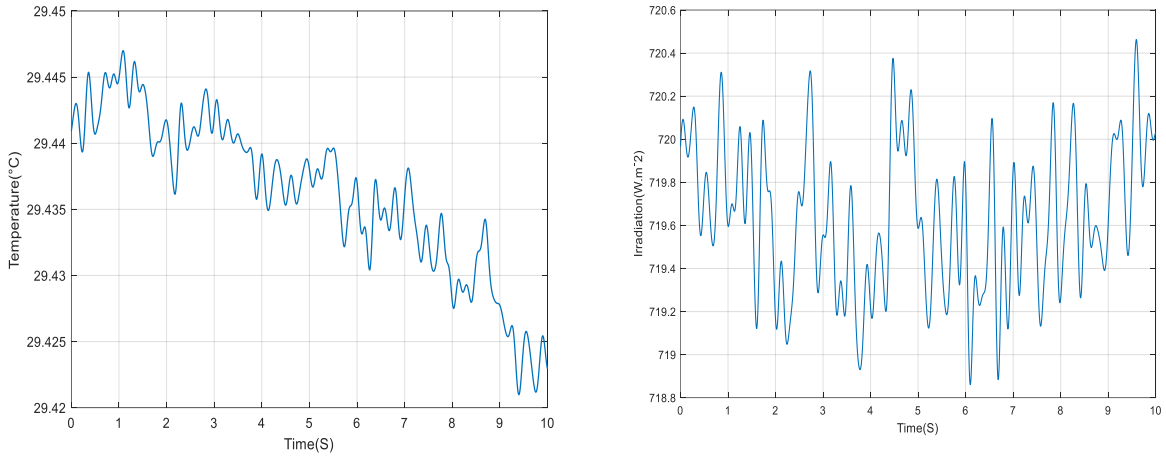

Figure 10. Solar irradiation and temperature profile.

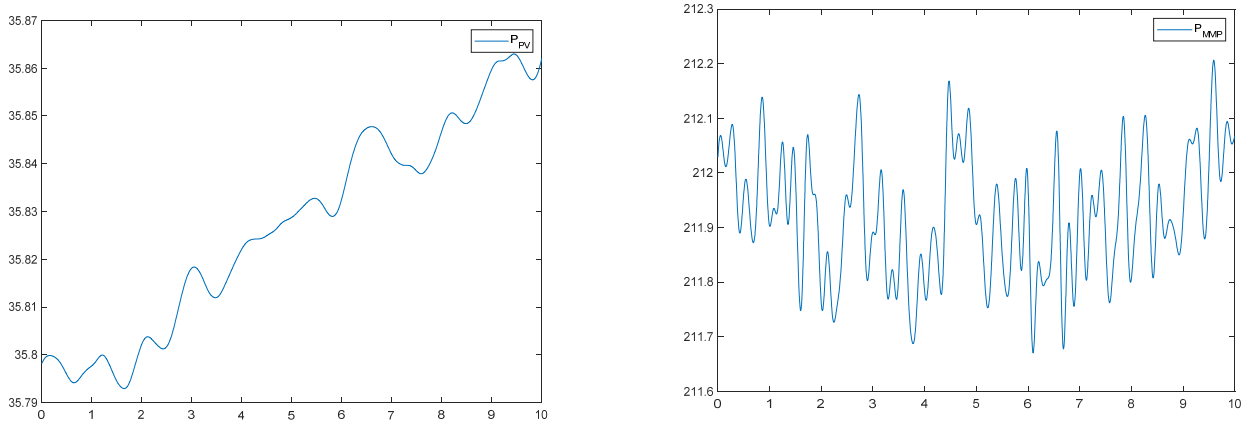

Figure 11. Optimization algorithm performance testing for PV.

Figure 12 illustrates the overall design. The effectiveness of the new neural-network-based prediction technique is evaluated by comparing the actual and predicted temperature and irradiation values, aiming to minimize the difference between the target and the predicted values.

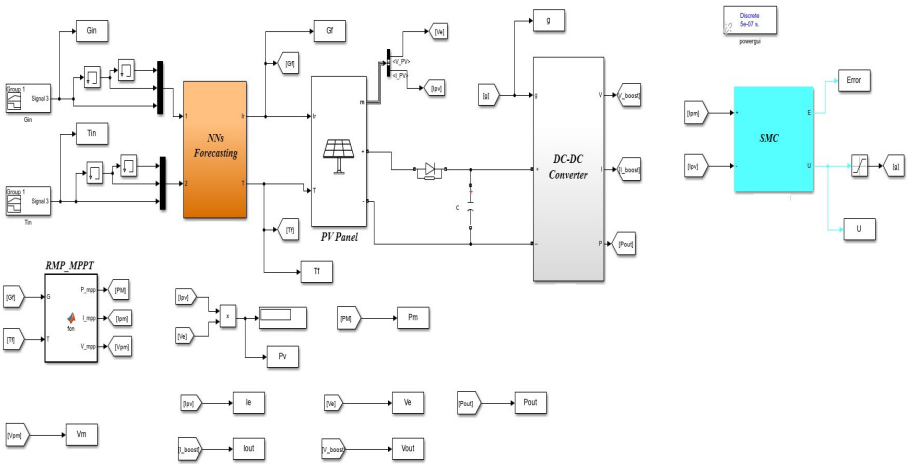

Figure 12. System's overall structure.

We used the predicted temperature and radiation (Tf and Gf) from Figure 13 to simulate the model and forecast the system's behavior under these conditions.

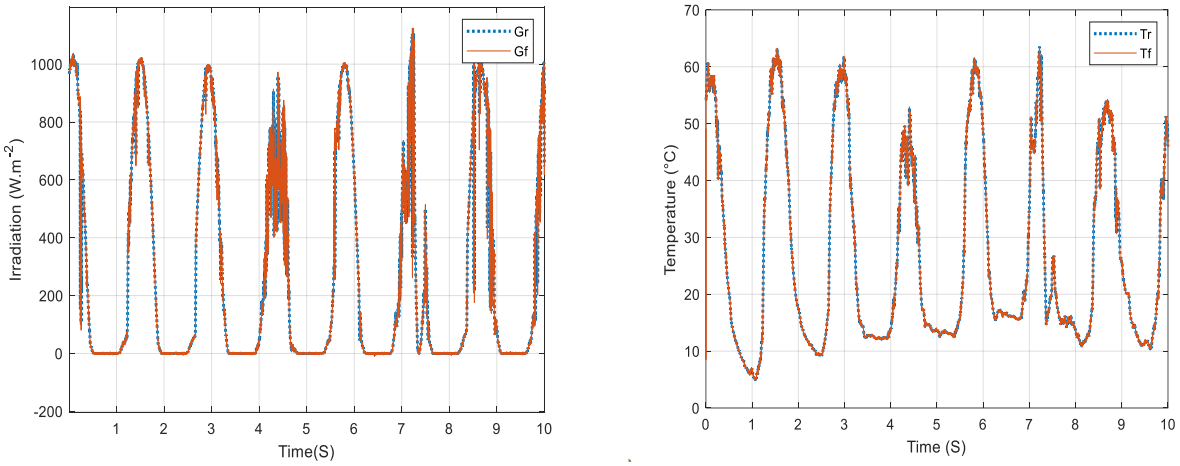

Figure 13. Irradiation and temperature profile.

Figure 14 shows the control signal and the error between the reference current (I_{mpp}) and the boost input current. The duty cycle changes along with the MPPT variations. This demonstrates the controller's ability to adjust to changing system conditions.

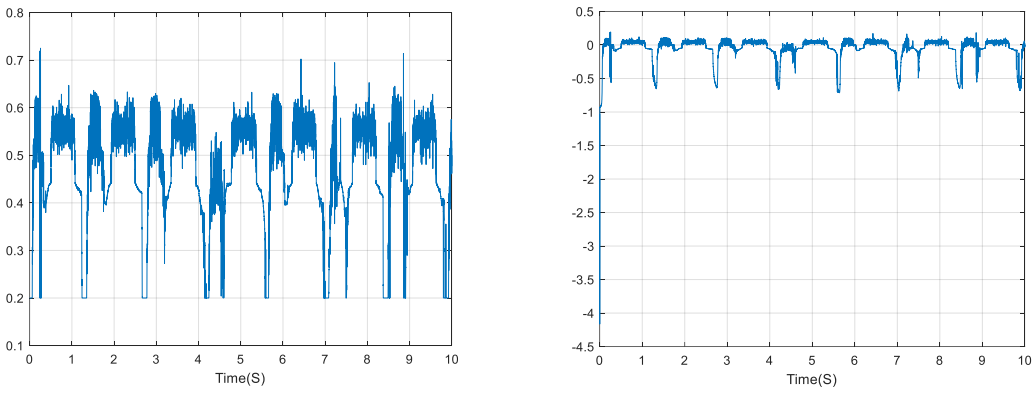

(**a**) (**b**)

Figure 14. Response of SMC: (**a**)controller signal; and (**b**) current error.

The small error shows that the SMC is accurate and effective in controlling the process. Figures 15–17 display, respectively, the voltage, current, and power results for our model, using a load with a resistance of 30 Ω.

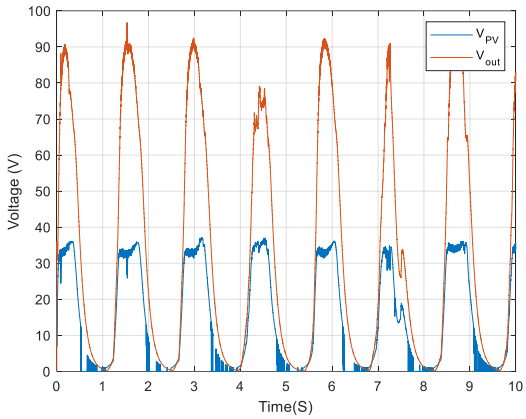

Figure 15. Temporal evolution of the voltage.

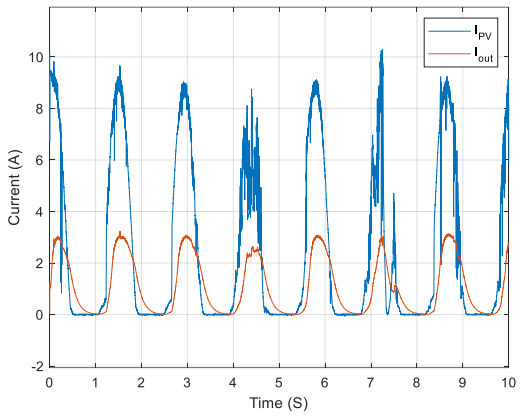

Figure 16. Temporal evolution of the electrical current.

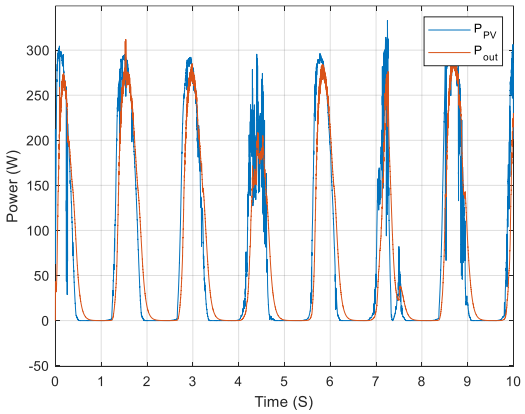

Figure 17. Temporal evolution of the power.

The previous figures demonstrate the optimization method's success in reaching the maximum point. The method adapts well to predicted changes, as seen in Figure 13. The SMC effectively tracks changes from both the optimizer and the PV panel, showing a strong performance during dynamic system transitions.

5. Comparative Study

5.1. Forecasting Method Comparison

To analyze the proposed forecasting solution, a comparative study was performed, and developed with specific time-series methodologies such as Autoregressive Moving Average (ARMA) and Autoregressive Integrated Moving Average (ARIMA). The results are shown in Figure 18 for the predictive temperatures and radiation values generated by each method.

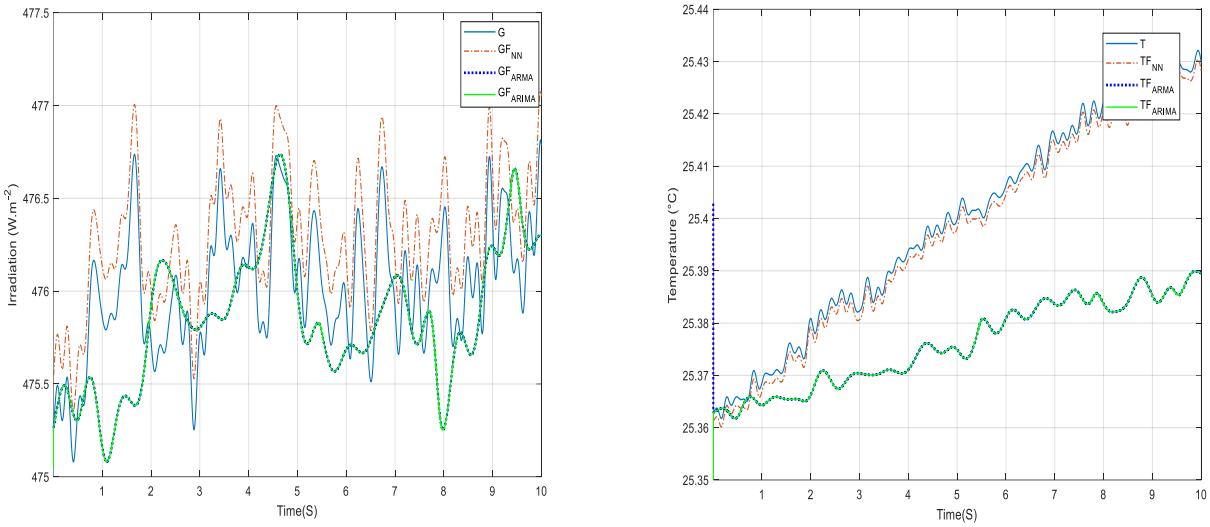

Figure 18. Comparative study of temperature and irradiation forecasting.

To evaluate the forecasting prowess of the ANN model, four metrics are employed, as illustrated in the equation below: R, Mean Absolute Error (MAE), Root Mean Square Error (RMSE), and MSE.

$$MAE = \frac{1}{n}\sum_{i=1}^{n}\left|y_{measured} - y_{predicted}\right| \quad (24)$$

$$MSE = \frac{1}{n}\sum_{i=1}^{n}\left(y_{measured} - y_{predicted}\right)^2 \quad (25)$$

$$RMSE = \sqrt{MSE} \quad (26)$$

$$R^2 = 1 - \frac{\sum\left(y_{measured} - y_{predicted}\right)^2}{\sum\left(y_{measured} - \overline{y}\right)^2} \quad (27)$$

where $\overline{y}$ is the mean value of $y_{measured}$

Table 1 presents analyses comparing our approach against recent studies in forecasting. We assess various aspects such as the system type and prediction model. This underscores the competitiveness of our methodology.

Table 1. Performance metric for prediction.

Model	R^2	MSE	RMSE	MAE	Neural N°	Training Data (%)
ANN	0.98	0.0044	0.066	0.033	15	70
ARIMA	0.99	0.29	0.47	0.088	-	70
ARMA	0.99	0.22	0.47	0.081	-	70

Based on Figure 18 and Table 1, it is clear that the artificial neural network stands out as the best performer among the models evaluated in terms of predictive accuracy. With an impressive R^2 score of 0.98, the proposed ANN model demonstrates a strong relationship between the predicted and actual values. The significantly low MSE of 0.0044, RMSE of 0.066, and MAE of 0.033 also confirm its accuracy and minimal forecast discrepancies. In

contrast, while the ARIMA and ARMA models show a strong correlation (R^2: 0.99), they show higher errors compared to ANN. Hence, the proposed ANN model outperforms the time-series-based approach in terms of accuracy and predictive ability.

ANNs outperform the ARIMA and ARMA models due to their ability to capture complex, non-linear patterns without strict assumptions about data distribution. They automatically learn relevant features from raw data, eliminating the need for manual feature engineering. This adaptability allows ANNs to effectively model time-series data with intricate dependencies and irregularities, making them versatile and powerful tools for forecasting. Additionally, ANNs generalize well to unseen data and can perform a wide range of tasks, enhancing their superiority over traditional statistical methods like ARIMA and ARMA.

5.2. MPPT Approach Comparison

To control the input current of the boost converter, we used the SMC, and, to verify the effectiveness of the proposed controller, we will compare it with one of the most famous classical controllers, which is the PI. Through experiments, we have determined the parameters of the PI controller, and the following Figures 19 and 20 show the comparison results of the controllers.

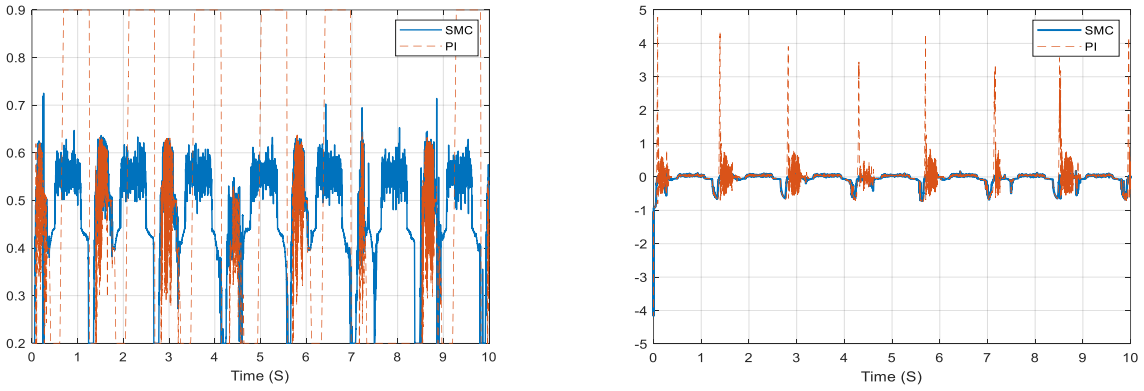

(**a**) (**b**)

Figure 19. Controller's response: (**a**) controller signal; and (**b**)current error.

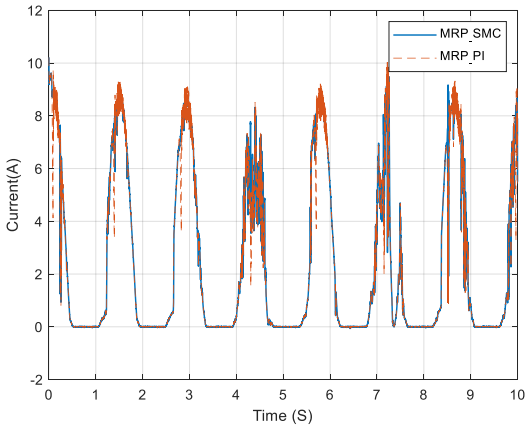

Figure 20. Comparison of the time evolution of PV current.

These figures show that the PI controller has some disadvantages compared to the SMC, especially when sudden changes occur. From Figure 19b, the SMC appears more stable and robust in handling the current error.

To enhance the evaluation of the proposed approach, a comprehensive comparative analysis was performed using the JAYA method. A brief overview of the JAYA algorithm is

provided in Appendix D for reference. In order to create a robust framework for evaluating performance, the following three figures illustrate the response of a PV system and serve as a basis for comparison. The Figure 21 shows the comparison between this two methods.

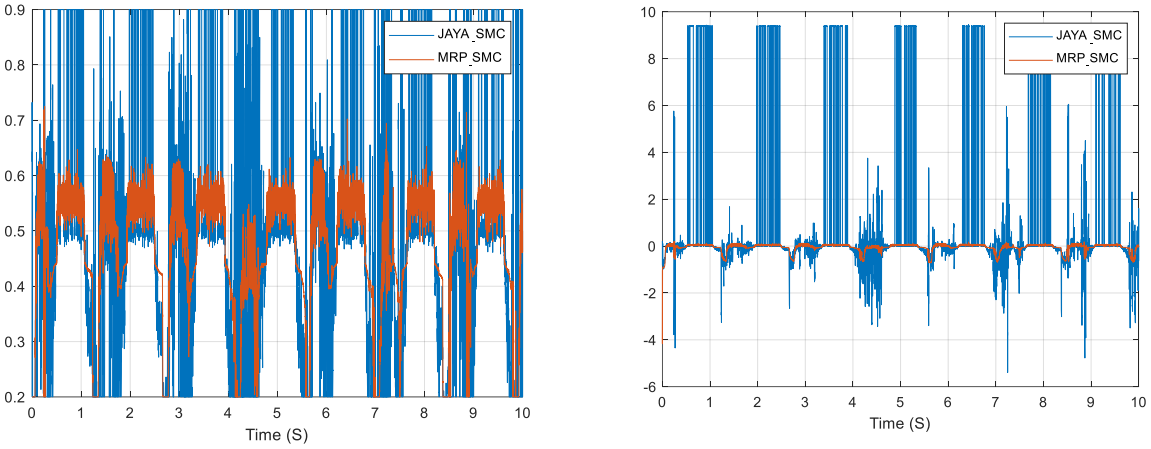

(**a**) (**b**)

Figure 21. Comparison of SMC response: (**a**) controller signal; and (**b**) current error.

From these two curves, we concluded that the SMC method performs better when used with the MRP method compared to the Jaya method. This is because MRP is faster in the MPP search, making SMC more stable, even with changes in error correction. Figures 22–24 show the time evolution comparison of the output voltage, current, and power, respectively.

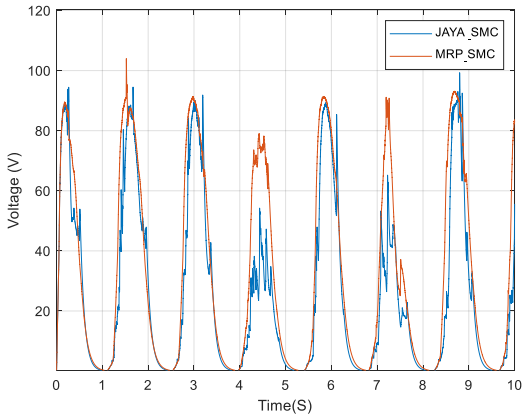

Figure 22. Comparison of the time evolution of output voltage.

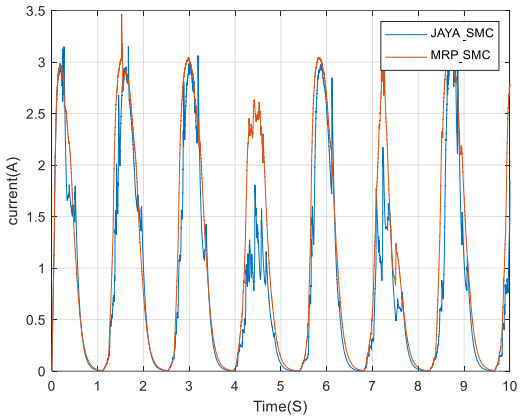

Figure 23. Comparison of the time evolution of output current.

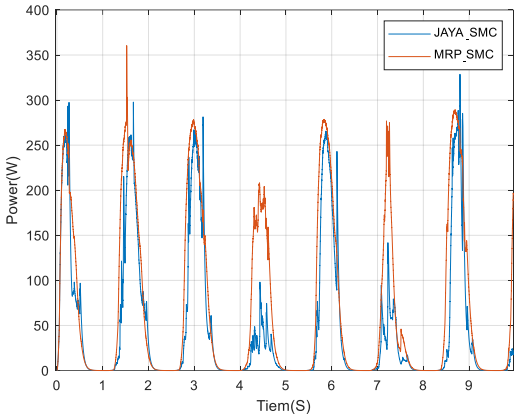

Figure 24. Comparison of the time evolution of output power.

The last three figures show that the MRP_SMC method outperforms JAYA_SMC by effectively tracking maximum points. Utilizing real-time temperature and radiation data in simulations, the MRP_SMC method exhibits superior adaptability to random variations, enabling it to identify maximum points more efficiently than JAYA_SMC. Conversely, JAYA struggles with rapid climate shifts, resulting in output fluctuations that can compromise the system's performance and accuracy, limiting its real-time applicability. In contrast, the MRP approach offers numerous advantages, including resilience to uncertainty, flexibility, support for risk-informed decision-making, integration with control strategies, and applicability across various domains. Additionally, the MRP method facilitates the quantification of uncertainty and provides enhanced decision support, making it invaluable for addressing optimization challenges in complex and uncertain environments.

6. Conclusions

In this study, we have introduced a new way to improve how we predict, control, and optimize the power output from solar panels. We use artificial neurons and a method called Minimal Risk Problem–Sliding Mode Control (MRP-SMC). Our method is efficient because it uses hidden layers to make better predictions and be more accurate. Unlike other methods, it can operate autonomously, even when errors occur or predictions are not perfect. Our method has been tested and shows good results. It has a low mean squared error (MSE) of 0.0044 and a high regression coefficient of 0.99, meaning it is very close to the actual output; the RMSE and MAE values are also low, showing that it predicts with minimal errors. We also use MRP-SMC to find and adjust the maximum power of the solar panels. Our method performs better than other methods like the JAYA method. It excels in adapting to weather-induced changes that impact solar panels. Our approach does not need extra equipment like Open-Circuit Voltage (OCV) or Short-Circuit Current (SCC) techniques. Instead, it controls the input current through the boost converter, using the reference Imp provided by the MRP. Our results show that our predictive model, MPPT, and SMC approaches are more effective than classical controllers. This is demonstrated by the comparison results between SMC and PI.

This research suggests future directions for improving MPPT in solar systems. We plan to develop a robust monitoring system and use intelligent systems to detect and rectify errors in real time.

Author Contributions: O.B.: conceptualization, simulation and data collection, and review. M.J.: simulation and data collection. M.J.: writing—original draft. M.J. and O.B.: writing—review and editing. F.H. and M.A.: supervision. All authors have read and agreed to the published version of the manuscript.

Funding: The authors wish to express their gratitude to the Basque Government, through the project EKOHEGAZ II (ELKARTEK KK-2023/00051); to the Diputación Foral de Álava (DFA), through the

project CONAVANTER; to the UPV/EHU, through the project GIU23/002; and to the Mobility Lab Foundation (CONV23/14, CONV23/12) for supporting this work.

Data Availability Statement: The original contributions presented in the study are included in the article, further inquiries can be directed to the corresponding authors.

Acknowledgments: I wish to extend my heartfelt appreciation to the individuals and organizations whose support and contributions have been pivotal in the completion of this article.

Conflicts of Interest: The authors declare no conflicts of interest.

Abbreviations

ANN	Artificial Neural Network
AI	Artificial Intelligence
NN	Neural Network
R	Regression
MSE	Mean Squared Error
MPP	Maximum Power Point
MPPT	Maximum Power Point Tracking
PV	Photovoltaic
P&O	Perturb and Observe
Tanh	Hyperbolic Tangent
OCV	Open-Circuit Voltage
SCC	Short-Circuit Current
SMC	Sliding Mode Control
GA	Genetic Algorithm
PSO	Particle Swarm Optimization
PI	Proportional Integral
DC	Direct Current
IC	Incremental Conductance
QSVM	Quadratic Support Vector Machine
CNN-BILSTM	Convolution Neural Network–Bi-Direction Long Short-Term Memory
ANFIS	Adaptive Neuron Fuzzy Inference System
GMDH	Group Method of Data Handling
ANFIS-PSO	Adaptive Neuron Fuzzy Inference System–Particle Swarm Optimization
SCG	Scaled Conjugate Gradient
SOP	Stochastic Optimization Problem

Appendix A. Sensor Specifications

Properties	Values
Voltage	12–28 V
Irradiance measurement range	Up to 1500 W/m^2
Temperature measurement range	−40 to 90 °C

Appendix B. PV Panel Parameters

Maximum power (Pmax)	340 W
Voltage at Pmax (Vmp)	36.7 V
Current at Pmax (Imp)	9.28 A
Open-circuit voltage (Voc)	45.2 V
Short circuit current (Isc)	9.9 A

Appendix C. The Boost Specifications

Properties	Values
Switching frequency	20 kHz
Maximum input voltage	60 V
Maximum output voltage	250 V
Maximum input current	30 A
Maximum output current	30 A

Appendix D. JAYA Algorithm

Step 1: Define the population size and the maximum number of iterations as N_{pop} and N_{max}, respectively.
Step 2: Identify the best and worst solutions as X_{best} and X_{worst}.
Step 3: While the current generation is less than or equal to N_{max}:

- For each individual in the population:
  - Update the individual's value using the equation $X_n(i,j) = X(i,j) + rand1_{i,j}(X_{best}(j) - |X(i,j)|) - rand2_{i,j}(X_{worst}(j) - |X(i,j)|)$
  - Assess the updated value and replace the previous one if it's more suitable.
  - End the loop.

Step 4: Display the existing solutions X(i) and their corresponding values f(X(i)).

References

1. Song, D.; Liu, Y.; Qin, T.; Gu, H.; Cao, Y.; Shi, H. Overview of the policy instruments for renewable energy development in China. *Energies* **2022**, *15*, 6513. [CrossRef]
2. Asif, M.H.; Zhongfu, T.; Ahmad, B.; Irfan, M.; Razzaq, A.; Ameer, W. Influencing factors of consumers' buying intention of solar energy: A structural equation modeling approach. *Environ. Sci. Pollut. Res.* **2023**, *30*, 30017–30032. [CrossRef] [PubMed]
3. Sarkar, D.; Odyuo, Y. An ab initio issues on renewable energy system integration to grid. *Int. J. Sustain. Energy Plan. Manag.* **2019**, *23*. [CrossRef]
4. Azarpour, A.; Mohammadzadeh, O.; Rezaei, N.; Zendehboudi, S. Current status and future prospects of renewable and sustainable energy in North America: Progress and challenges. *Energy Convers. Manag.* **2022**, *269*, 115945. [CrossRef]
5. Katche, M.L.; Makokha, A.B.; Zachary, S.O.; Adaramola, M.S. A comprehensive review of maximum power point tracking (mppt) techniques used in solar pv systems. *Energies* **2023**, *16*, 2206. [CrossRef]
6. Nkambule, M.S.; Hasan, A.N.; Ali, A.; Hong, J.; Geem, Z.W. Comprehensive evaluation of machine learning MPPT algorithms for a PV system under different weather conditions. *J. Electr. Eng. Technol.* **2021**, *16*, 411–427. [CrossRef]
7. Verma, D.; Nema, S.; Agrawal, R.; Sawle, Y.; Kumar, A. A different approach for maximum power point tracking (MPPT) using impedance matching through non-isolated DC-DC converters in solar photovoltaic systems. *Electronics* **2022**, *11*, 1053. [CrossRef]
8. Khodair, D.; Motahhir, S.; Mostafa, H.H.; Shaker, A.; Munim, H.A.E.; Abouelatta, M.; Saeed, A. Modeling and Simulation of modified MPPT techniques under varying operating climatic conditions. *Energies* **2023**, *16*, 549. [CrossRef]
9. Radia, M.A.; El Nimr, M.K.; Atlam, A.S. IoT-based wireless data acquisition and control system for photovoltaic module performance analysis. *E-Prime-Adv. Electr. Eng. Electron. Energy* **2023**, *6*, 100348. [CrossRef]
10. Rojek, I.; Mikołajewski, D.; Mroziński, A.; Macko, M. Machine Learning-and Artificial Intelligence-Derived Prediction for Home Smart Energy Systems with PV Installation and Battery Energy Storage. *Energies* **2023**, *16*, 6613. [CrossRef]
11. Sharma, A.K.; Pachauri, R.K.; Choudhury, S.; Minai, A.F.; Alotaibi, M.A.; Malik, H.; Márquez, F.P.G. Role of metaheuristic approaches for implementation of integrated MPPT-PV systems: A comprehensive study. *Mathematics* **2023**, *11*, 269. [CrossRef]
12. Mehazzem, F.; André, M.; Calif, R. Efficient Output Photovoltaic Power Prediction Based on MPPT Fuzzy Logic Technique and Solar Spatio-Temporal Forecasting Approach in a Tropical Insular Region. *Energies* **2022**, *15*, 8671. [CrossRef]
13. Koeva, D.; Kutkarska, R.; Zinoviev, V. High Penetration of Renewable Energy Sources and Power Market Formation for Countries in Energy Transition: Assessment via Price Analysis and Energy Forecasting. *Energies* **2023**, *16*, 7788. [CrossRef]
14. Gielen, D.; Boshell, F.; Saygin, D.; Bazilian, M.D.; Wagner, N.; Gorini, R. The role of renewable energy in the global energy transformation. *Energy Strategy Rev.* **2019**, *24*, 38–50. [CrossRef]
15. Sajid, I.; Gautam, A.; Sarwar, A.; Tariq, M.; Liu, H.D.; Ahmad, S.; Sayed, A.E. Optimizing Photovoltaic Power Production in Partial Shading Conditions Using Dandelion Optimizer (DO)-Based MPPT Method. *Processes* **2023**, *11*, 2493. [CrossRef]
16. Akman, D.V.; Malekipirbazari, M.; Yenice, Z.D.; Yeo, A.; Adhikari, N.; Wong, Y.K.; Gumus, A.T. k-best feature selection and ranking via stochastic approximation. *Expert Syst. Appl.* **2023**, *213*, 118864. [CrossRef]

17. Triki, Y.; Bechouche, A.; Seddiki, H.; Abdeslam, D.O. An improved incremental conductance based MPPT algorithm for photovoltaic systems. In Proceedings of the IECON 2021–47th Annual Conference of the IEEE Industrial Electronics Society, Toronto, ON, Canada, 13–16 October 2021; pp. 1–6. [CrossRef]
18. Thirunavukkarasu, G.S.; Seyedmahmoudian, M.; Jamei, E.; Horan, B.; Mekhilef, S.; Stojcevski, A. Role of optimization techniques in microgrid energy management systems—A review. *Energy Strategy Rev.* **2022**, *43*, 100899. [CrossRef]
19. Du, Y.; Xu, F. A hybrid multi-step probability selection particle swarm optimization with dynamic chaotic inertial weight and acceleration coefficients for numerical function optimization. *Symmetry* **2020**, *12*, 922. [CrossRef]
20. Jlidi, M.; Hamidi, F.; Abdelkrim, M.N.; Jerbi, H.; Abbassi, R.; Kchaou, M. Synthesis of an Advanced Maximum Power Point Tracking Method for a Photovoltaic System: A Chaotic Jaya Logistic Approach. In Proceedings of the 2022 4th International Conference on Applied Automation and Industrial Diagnostics (ICAAID), Hail, Saudi Arabia, 29–31 March 2022; pp. 1–6. [CrossRef]
21. Chaitanya, K.; Somayajulu, D.V.; Krishna, P.R. Memory-based approaches for eliminating premature convergence in particle swarm optimization. *Appl. Intell.* **2021**, *51*, 4575–4608. [CrossRef]
22. Alshammari, B.M.; Farah, A.; Alqunun, K.; Guesmi, T. Robust design of dual-input power system stabilizer using chaotic Jaya algorithm. *Energies* **2021**, *14*, 5294. [CrossRef]
23. Yang, J.; Hu, Y.; Zhang, K.; Wu, Y. An improved evolution algorithm using population competition genetic algorithm and self-correction BP neural network based on fitness landscape. *Soft Comput.* **2021**, *25*, 1751–1776. [CrossRef]
24. Zafar, M.H.; Khan, N.M.; Mirza, A.F.; Mansoor, M.; Akhtar, N.; Qadir, M.U.; Moosavi, S.K.R. A novel meta-heuristic optimization algorithm based MPPT control technique for PV systems under complex partial shading condition. *Sustain. Energy Technol. Assess.* **2021**, *47*, 101367. [CrossRef]
25. Colbu, Ş.C.; Popescu, D.; Băncilă, D.M.; Mone, M.A.; Petrescu-Niţă, A. Stochastic Optimization and Risk Problems for Engineering Applications. In Proceedings of the 2022 8th International Conference on Control, Decision and Information Technologies (CoDIT), Istanbul, Turkey, 17–20 May 2022; pp. 775–779. [CrossRef]
26. Ampountolas, A. Modeling and forecasting daily hotel demand: A comparison based on sarimax, neural networks, and garch models. *Forecasting* **2021**, *3*, 580–595. [CrossRef]
27. Kurani, A.; Doshi, P.; Vakharia, A.; Shah, M. A comprehensive comparative study of artificial neural network (ANN) and support vector machines (SVM) on stock forecasting. *Ann. Data Sci.* **2023**, *10*, 183–208. [CrossRef]
28. Gourvenec, S.; Sturt, F.; Reid, E.; Trigos, F. Global assessment of historical, current and forecast ocean energy infrastructure: Implications for marine space planning, sustainable design and end-of-engineered-life management. *Renew. Sustain. Energy Rev.* **2022**, *154*, 111794. [CrossRef]
29. Acharya, S.K.; Wi, Y.M.; Lee, J. Day-ahead forecasting for small-scale photovoltaic power based on similar day detection with selective weather variables. *Electronics* **2020**, *9*, 1117. [CrossRef]
30. Ellahi, M.; Usman, M.R.; Arif, W.; Usman, H.F.; Khan, W.A.; Satrya, G.B.; Shabbir, N. Forecasting of Wind Speed and Power through FFNN and CFNN Using HPSOBA and MHPSO-BAACs Techniques. *Electronics* **2022**, *11*, 4193. [CrossRef]
31. Jlidi, M.; Hamidi, F.; Barambones, O.; Abbassi, R.; Jerbi, H.; Aoun, M.; Karami-Mollaee, A. An Artificial Neural Network for Solar Energy Prediction and Control Using Jaya-SMC. *Electronics* **2023**, *12*, 592. [CrossRef]
32. Kabilan, R.; Chandran, V.; Yogapriya, J.; Karthick, A.; Gandhi, P.P.; Mohanavel, V.; Manoharan, S. Short-term power prediction of building integrated photovoltaic (BIPV) system based on machine learning algorithms. *Int. J. Photoenergy* **2021**, *2021*, 5582418. [CrossRef]
33. Rai, A.; Shrivastava, A.; Jana, K.C. A CNN-BiLSTM based deep learning model for mid-term solar radiation prediction. *Int. Trans. Electr. Energy Syst.* **2021**, *31*, e12664. [CrossRef]
34. Obiora, C.N.; Ali, A.; Hasan, A.N. Estimation of hourly global solar radiation using deep learning algorithms. In Proceedings of the 2020 11th International Renewable Energy Congress (IREC), Hammamet, Tunisia, 29–31 October 2020; pp. 1–6. [CrossRef]
35. Olatomiwa, L.; Mekhilef, S.; Shamshirband, S.; Petković, D. Adaptive neuro-fuzzy approach for solar radiation prediction in Nigeria. *Renew. Sustain. Energy Rev.* **2015**, *51*, 1784–1791. [CrossRef]
36. Khosravi, A.; Nunes, R.O.; Assad, M.E.H.; Machado, L. Comparison of artificial intelligence methods in estimation of daily global solar radiation. *J. Clean. Prod.* **2018**, *194*, 342–358. [CrossRef]
37. Halabi, L.M.; Mekhilef, S.; Hossain, M. Performance evaluation of hybrid adaptive neuro-fuzzy inference system models for predicting monthly global solar radiation. *Appl. Energy* **2018**, *213*, 247–261. [CrossRef]
38. Yilmaz, U.; Kircay, A.; Borekci, S. PV system fuzzy logic MPPT method and PI control as a charge controller. *Renew. Sustain. Energy Rev.* **2018**, *81*, 994–1001. [CrossRef]
39. Idrissi, Y.E.A.; Assalaou, K.; Elmahni, L.; Aitiaz, E. New improved MPPT based on artificial neural network and PI controller for photovoltaic applications. *Int. J. Power Electron. Drive Syst.* **2022**, *13*, 1791. [CrossRef]
40. Tang, J.; Ni, H.; Peng, R.L.; Wang, N.; Zuo, L. A review on energy conversion using hybrid photovoltaic and thermoelectric systems. *J. Power Sources* **2023**, *562*, 232785. [CrossRef]
41. Geethamahalakshmi, G.; Kalaiarasi, N.; Nageswari, D. Fuzzy based MPPT and solar power forecasting using artificial intelligence. *Intell. Autom. Soft Comput.* **2022**, *32*, 1667–1685. [CrossRef]
42. Hamidi, F.; Olteanu, S.C.; Popescu, D.; Jerbi, H.; Dincă, I.; Ben Aoun, S.; Abbassi, R. Model Based Optimisation Algorithm for Maximum Power Point Tracking in Photovoltaic Panels. *Energies* **2020**, *13*, 4798. [CrossRef]

43. Al-Masri, H.M.; Magableh, S.K.; Abuelrub, A.; Saadeh, O.; Ehsani, M. Impact of different photovoltaic models on the design of a combined solar array and pumped hydro storage system. *Appl. Sci.* **2020**, *10*, 3650. [CrossRef]
44. Nguyen-Duc, T.; Nguyen-Duc, H.; Le-Viet, T.; Takano, H. Single-diode models of PV modules: A comparison of conventional approaches and proposal of a novel model. *Energies* **2020**, *13*, 1296. [CrossRef]
45. Rusirawan, D.; Farkas, I. Identification of model parameters of the photovoltaic solar cells. *Energy Procedia* **2014**, *57*, 39–46. [CrossRef]
46. Anani, N.; Ibrahim, H. Adjusting the single-diode model parameters of a photovoltaic module with irradiance and temperature. *Energies* **2020**, *13*, 3226. [CrossRef]
47. Escamilla-García, A.; Soto-Zarazúa, G.M.; Toledano-Ayala, M.; Rivas-Araiza, E.; Gastélum-Barrios, A. Applications of artificial neural networks in greenhouse technology and overview for smart agriculture development. *Appl. Sci.* **2020**, *10*, 3835. [CrossRef]
48. Sajjad, U.; Hussain, I.; Raza, W.; Sultan, M.; Alarifi, I.M.; Wang, C.C. On the critical heat flux assessment of micro-and nanoscale roughened surfaces. *Nanomaterials* **2022**, *12*, 3256. [CrossRef]
49. Gaspar, A.; Oliva, D.; Cuevas, E.; Zaldívar, D.; Pérez, M.; Pajares, G. Hyperparameter optimization in a convolutional neural network using metaheuristic algorithms. In *Metaheuristics in Machine Learning: Theory and Applications*; Springer International Publishing: Cham, Switzerland, 2021; pp. 37–59. [CrossRef]